

Optimal EPI parameters for reduction of susceptibility-induced BOLD sensitivity losses: A whole-brain analysis at 3 T and 1.5 T

Nikolaus Weiskopf,* Chloe Hutton, Oliver Josephs, and Ralf Deichmann

Wellcome Department of Imaging Neuroscience, Institute of Neurology, University College London, London, WC1N 3BG, UK

Received 24 April 2006; revised 16 July 2006; accepted 18 July 2006
Available online 7 September 2006

Most functional magnetic resonance imaging (fMRI) studies record the blood oxygen level-dependent (BOLD) signal using fast gradient-echo echo-planar imaging (GE EPI). However, GE EPI can suffer from substantial signal dropout caused by inhomogeneities in the static magnetic field. These field inhomogeneities occur near air/tissue interfaces, because they are generated by variations in magnetic susceptibilities. Thus, fMRI studies are often limited by a reduced BOLD sensitivity (BS) in inferior brain regions. Recently, a method has been developed which allows for optimizing the BS in dropout regions by specifically adjusting the slice tilt, the direction of the phase-encoding (PE), and the z-shim moment. However, optimal imaging parameters were only reported for the orbitofrontal cortex (OFC) and inferior temporal lobes. The present study determines the optimal slice tilt, PE direction, and z-shim moment at 3 T and 1.5 T, otherwise using standard fMRI acquisition parameters. Results are reported for all brain regions, yielding a whole-brain atlas of optimal parameters. At both field strengths, optimal parameters increase the BS by more than 60% in many voxels in the OFC and by at least 30% in the other dropout regions. BS gains are shown to be more widespread at 3 T, suggesting an increased benefit from the dropout compensation at higher fields. Even the mean BS of a large brain region, e.g., encompassing the medial OFC, can be increased by more than 15%. The maps of optimal parameters allow for assessing the feasibility and improving fMRI of brain regions affected by susceptibility-induced BS losses.

© 2006 Elsevier Inc. All rights reserved.

Keywords: Signal loss; Susceptibility artifacts; EPI; fMRI; BOLD sensitivity; z-shim

Introduction

Gradient-echo echo-planar imaging (GE EPI) is widely used for functional magnetic resonance imaging (fMRI) of the brain (Moonen and Bandettini, 2000). GE EPI is sensitive to microscopic

magnetic field alterations caused by blood oxygen level-dependent (BOLD) susceptibility effects indicating neuronal activity (Logothetis, 2003). However, it is also sensitive to the macroscopic field inhomogeneities caused by the differences of magnetic susceptibility of air and tissue which may result in local image distortions and signal losses. While the image distortions may be corrected by various on-line and off-line methods (e.g., Andersson et al., 2001; Bowtell et al., 1994; Hutton et al., 2002; Jezzard and Balaban, 1995; Sutton et al., 2004; Weiskopf et al., 2005b; Zaitsev et al., 2004), signal dropouts have often compromised fMRI studies of the inferior frontal, the medial temporal and the inferior temporal lobes (Devlin et al., 2000; Merboldt et al., 2001; Ojemann et al., 1997).

Several methods have been devised for reducing susceptibility-related signal losses. Resistive shim coils have been used to homogenize the magnetic field (Hsu and Glover, 2005). However, strong magnetic field inhomogeneities can only be counterbalanced by shimming a relatively small volume or relatively small spatial orders. Signal losses may be reduced by using tailored radio-frequency (RF) pulses for excitation, opposing the dephasing effect of the susceptibility related field gradients. However, quadratic phase profile RF pulses reduce the signal-to-noise ratio (SNR) in well-shimmed brain areas (Cho and Ro, 1992). Three-dimensional tailored RF pulses are very long and require individual design of the RF pulse for each subject before the fMRI experiment (Stenger et al., 2000), a facility not yet readily available on standard scanners. In general, in all directions smaller voxel sizes reduce the signal loss but only at the expense of a reduced SNR in well-shimmed areas (Merboldt et al., 2000).

Z-shimming is a widely used compensation technique. A series of images with different compensation gradient prepulses, counteracting the susceptibility-induced gradient in the slice selection direction, is acquired and combined (e.g., Cordes et al., 2000; Frahm et al., 1988; Ordidge et al., 1994). This method has been extended to the phase encoding (PE) direction by Deichmann et al. (2002). Although these methods can almost fully recover signal losses, they significantly reduce the temporal resolution. Thus, they compromise many fMRI studies requiring a high temporal resolution, such as connectivity measurements (Friston et al., 2003; Roebroeck et al., 2005) or event-related studies (Josephs et

* Corresponding author. Fax: +44 20 7813 1420.

E-mail address: n.weiskopf@fil.ion.ucl.ac.uk (N. Weiskopf).

Available online on ScienceDirect (www.sciencedirect.com).

al., 1997). A faster technique using optimal slice tilts (Deichmann et al., 2003) and PE directions (De Panfilis and Schwarzbauer, 2005) combined with a moderate z-shim gradient prepulse has been developed. The z-shimming gradient counteracts susceptibility-induced through-plane gradients whilst the slice tilt is used to orient the slice so that the susceptibility-induced gradient in the PE direction is small enough not to cause dropouts. The polarity of the PE gradient can also be chosen optimally. These techniques, combined together, have been shown to considerably enhance the BOLD sensitivity (BS) in the orbitofrontal cortex (OFC; Deichmann et al., 2003) and inferior temporal lobes (De Panfilis and Schwarzbauer, 2005) whilst only slightly decreasing the BS in well-shimmed areas. Since this approach only requires a single acquisition, the high temporal resolution of standard EPI can be retained.

We aimed to create 3D maps showing the scanning parameters which optimize the BS for each voxel across the whole brain. In contrast to previous works on the same subject which focused on the OFC and the inferior temporal lobes, these maps allow for an informed choice of the slice tilt, z-shim gradient moment, and PE gradient polarity in all brain regions. To provide data, we scanned a group of 5 subjects, varying systematically the slice tilt, the z-shim gradient moment, and the PE gradient polarity. We scanned at two commonly used field strengths of 3 T and 1.5 T using otherwise standard fMRI imaging parameters. We estimated the local BS for the group according to Deichmann et al. (2002) based on the complex EPI raw data. We determined the maximal achievable BS and respective optimal imaging parameters for each brain region given that the z-shimming prepulse should not reduce the BS in well-shimmed areas by more than 15%. To aid the decision about which field strength should be used for scanning particular regions of interest, we located regions where the BS achievable at 3 T differed significantly from that at 1.5 T, when optimal parameter sets have been chosen for each field strength.

Methods

Data acquisition and image processing

Five volunteers (1 female, 4 male, age 29–36 years) were scanned in both a 1.5 T whole-body scanner (Magnetom Sonata, Siemens Medical, Erlangen, Germany) and a 3 T head scanner (Magnetom Allegra, Siemens Medical). The whole-body scanner was operated with its standard body transmit and head receive coil (single receive CP head array), the head scanner with its standard birdcage transmit-receive coil. All volunteers gave written consent as required by the local ethics committee. The participants were scanned in supine position.

The manufacturer's standard automatic 3D-shim procedure was performed at the beginning of each experiment, to correct for first and second order distortions in the static magnetic field in a given adjust volume. The adjust volume corresponded to the volume covered by the EPI imaging volume recorded with a slice tilt of $\beta = -30^\circ$ (for imaging details see below). The participants were scanned with a single-shot EPI sequence which allowed for the free choice of the moment of the z-shimming gradient prepulse (M_z^{comp}) and the PE gradient polarity. The EPI imaging parameters at 1.5 T/3 T were: 48 oblique transverse slices, slice thickness=2 mm, gap between slices=1 mm, repetition time $TR=4.3/3.1$ s, $\alpha=90^\circ$, echo time $TE=50/30$ ms, bandwidth $BW=2298/3551$ Hz/pixel, bandwidth in PE direction $BW_{PE}=31.3/47.3$ Hz/pixel, PE direction

anterior–posterior, field of view $FOV=192 \times 192$ mm², matrix size 64×64 . The z-shimming gradient moment was varied from $M_z^{\text{comp}}=-4$ mT/m ms to $+4$ mT/m ms (in 9 steps of 1 mT/m ms), the slice tilt from $\beta=-45^\circ$ to $+30^\circ$ (in 6 steps of 15°), and the PE gradient was set to either positive or negative polarity, resulting in 108 different parameter combinations. The slice tilt β is defined as the angle of the rotation (pitch) about the x-axis/left–right scanner axis measured from the axial plane (=plane defined by the left–right and the vertical scanner axis), with positive values denoting tilts of the anterior edge of the slice towards the feet. A positive PE gradient polarity corresponds to a positive PE prewinder moment, i.e., the respective gradient points from the posterior to the anterior part of the brain. For each parameter combination a short time-series of 5 EPI volumes was acquired. Further analysis was based on the last volume of the time-series to exclude transitional T_1 saturation effects. At 3 T, a posthoc analysis of the BS in brain areas not affected by susceptibility-induced field inhomogeneities showed that the data acquired at $TE=30$ ms was subject to a residual z-gradient moment of 0.6 mT/m ms. This effect may be due to either a slight offset of the z-gradient caused by the shim coil or a miscalibration of the slice refocusing gradient. Therefore, the effective z-shimming gradient moments at 3 T were $+0.6$ mT/m ms higher than the nominal values, i.e., effectively ranging from -3.4 mT/m ms to $+4.6$ mT/m ms. In the following, all reported z-shimming moments are the effective values. Although data were acquired at a comprehensive range of z-shimming gradient moments, those exceeding ± 2.5 mT/m ms were not included in the further analysis, because according to the theory (Deichmann et al., 2003) they cause significant BS loss ($>15\%$) in well-shimmed areas at a slice thickness of 2 mm.

EPI magnitude images, echo time (TE) maps, and BS maps were reconstructed from the complex k-space data using a generalized reconstruction method based on the measured EPI k-space trajectory to minimize ghosting (Josephs et al., 2000). The TE maps and BS maps were estimated according to Deichmann et al. (2002). The BS was determined from the product of the image intensity I and local TE: $BS=TE \times I$. The image intensity was extracted from the magnitude of the complex reconstructed image. The local TE was determined from the local phase increment across lines (in the PE direction) in the complex image: $TE=TE_0 + (TE_0 - t_0)\Delta\Phi/\pi$, with TE_0 being the nominal echo time as entered on the scanner interface, t_0 being the time difference between RF excitation and the start of the EPI readout, and $\Delta\Phi$ being the phase increment per line in the PE direction in the complex image. A detailed derivation of the calculation of BS and TE can be found in the Theory section and the Appendix C in Deichmann et al. (2002).

For anatomical reference and spatial normalization, a high-resolution T_1 -weighted 3D image was acquired for each participant at 1.5 T (3D MDEFT [Deichmann et al., 2004]; $FOV=256 \times 224$ mm² or 256×240 mm², matrix size 256×224 or 256×240 , 176 partitions, slab thickness 176 mm, $\tau_1=222.6$ ms, $\tau_2=307.4$ ms, $TR=12.24$ ms, $TE=3.56$ ms, $\alpha=23^\circ$, $BW=106$ Hz/pixel). For each experiment, a field map using a double echo FLASH sequence was recorded for distortion correction. The parameters at 1.5 T/3 T were: 64 oblique transverse slices, slice thickness=2 mm, gap between slices=1 mm, $TR=1170/1020$ ms, $\alpha=90^\circ$, short $TE=10$ ms, long $TE=14.76/12.46$ ms, $BW=260$ Hz/pixel, PE direction anterior–posterior, $FOV=192 \times 192$ mm², matrix size 64×64 , flow compensation). In one subject, only 48 slices were sufficient to record the whole head field map (reduced $TR=874/$

761 ms [1.5 T/3 T]). In one other experiment (at 1.5 T) the field map was recorded with an increased matrix size of 128×128 and $FOV = 210 \times 210 \text{ mm}^2$ to avoid wrap over in the PE direction (slice thickness = 2 mm, gap = 0.4 mm). Other imaging parameters were adjusted accordingly.

Using the FieldMap toolbox (Hutton et al., 2002, 2004), field maps were estimated from the phase difference between the images acquired at the short and long TE. After spatial smoothing of the field map (Gaussian kernel, FWHM = 6 mm), voxel displacements in the EPI image were determined from the fieldmap and given imaging parameters. Unwarping was performed by applying the inverse displacement to the EPI magnitude images, TE maps, and BS maps without a correction for the distortion-induced intensity modulations. This correction was omitted, because it can reduce the signal-to-noise ratio (SNR; Hutton et al., 2002). The T_1 -weighted 3D image, field maps, and all images derived from EPI (magnitude, TE, BS) were coregistered, resliced, and spatially normalized using SPM2 (Ashburner and Friston, 1999; Friston et al., 1995). The estimation of the parameters of the non-linear spatial normalization was based on matching the individual T_1 -weighted 3D image to the 152 brains template (Collins et al., 1994) supplied by the Montreal Neurological Institute (MNI). For the group analysis, the BS maps were masked to exclude non-brain areas and areas not scanned in all subjects (by the inclusive conjunction of the imaging volumes and the MNI template brain mask) and spatially smoothed (Gaussian kernel, FWHM = 6 mm).

Maps: BS, BS gain, and optimal EPI parameters

A baseline BS map for each subject was determined from the standard EPI acquisition (with slice tilt $\beta = 0^\circ$, minimal effective z-shimming moment $M_z^{\text{comp}} = 0 \text{ mT/m ms}$ at 1.5 T and $M_z^{\text{comp}} = -0.4 \text{ mT/m*ms}$ at 3 T, and a positive PE gradient polarity). To allow for easier interpretation, each subject's BS map was scaled to 100% for the mean BS value in well-shimmed brain areas of the baseline BS map. The well-shimmed brain areas were defined as the supplementary motor area (SMA), paracentral lobules, precentral gyri, postcentral gyri, and the superior parietal gyri identified according to the automated anatomical labeling toolbox (AAL; Tzourio-Mazoyer et al., 2002).

For each voxel, we determined the mean BS across the group for each acquisition parameter set. The optimal EPI acquisition parameters (β , M_z^{comp} , PE gradient polarity) yielding the highest mean BS were selected, excluding z-shimming moments yielding a BS loss higher than 15% in well-shimmed areas ($|M_z^{\text{comp}}| < 2.5 \text{ mT/m ms}$). These parameters produced an optimal BS map. The gain in BS using optimal acquisition parameters was calculated by subtracting the baseline BS map from the optimal BS map.

The BS maps are in relative rather than absolute units. To allow for a comparison between field strengths, we assumed that the BS should increase by approximately 20% in well-shimmed areas going from 1.5 T to 3 T in an fMRI group study. This figure is a conservative estimate based on studies comparing temporal SNR (Triantafyllou et al., 2005) and BOLD CNR (Hoenig et al., 2005; Turner et al., 2005) at 1.5 T and 3 T. All maps except for the maximal BS maps were thresholded at a BS gain of 15%, to focus on the areas where the dropout compensation significantly improved the BS. For anatomical reference, all maps were superimposed over the group averaged T_1 -weighted anatomical image.

Region of interest analysis: optimal EPI parameters for a brain region

In addition to selecting optimal parameters for each voxel, we calculated the optimal parameter set for a selection of extended brain regions which are frequently studied: namely, the medial orbitofrontal cortex (mOFC) and rostral-ventral anterior cingulate cortex (rACC) as the part of the OFC and ACC suffering most from dropouts (orbital and medial orbital part of the superior frontal gyri, olfactory cortex, gyrus rectus, anterior cingulate with $z < 0$); the inferior temporal gyri; temporal poles (superior and mid temporal pole); amygdala; and hippo- and parahippocampal region. All regions of interest were extracted from the AAL toolbox (Tzourio-Mazoyer et al., 2002), except for the amygdala region which was defined by a cytoarchitectonic probability map ($p > 10\%$) described by Amunts et al. (2005) using the SPM Anatomy toolbox (Eickhoff et al., 2005). For each region we determined the parameter set maximizing the mean BS across all voxels in the region. To assess the inter-subject variation, the optimization was performed both for the group mean and for each subject individually.

Results

The head orientation of the subjects in each scanner differed only minimally. The largest deviations were observed in the rotation (pitch) about the left–right axis (the pitch was measured as the angle between the scanner's vertical axis and the AC–PC line approximated by the $x = 0, z = 0$ line in MNI space). In the 3 T scanner the pitch was on average $-14.9^\circ \pm 4.1^\circ$ (mean \pm standard deviation), and in the 1.5 T scanner $-10.8^\circ \pm 4.0^\circ$.

Maps: BS, BS gain, and optimal EPI parameters

The BS and derived maps are shown in Fig. 1. Fig. 1a shows that optimal imaging parameters increased the BS by more than 15% compared to the baseline BS in many brain regions inferior to the anterior commissure ($z = 0 \text{ mm}$). The maximal gains in BS exceeded 60% at both field strengths. The gains in BS, however, were more widespread at 3 T. Despite this increase in BS, inferior frontal and temporal areas suffered a persistent dropout (e.g., the U-shaped region at $z = -24 \text{ mm}$ in Fig. 1b). As shown in Fig. 1c, in the great majority of areas affected by signal dropout, higher BS was observed for 3 T than 1.5 T. Only a small part of the left inferior temporal gyrus (Fig. 1c, $z = -36 \text{ mm}$) showed a higher BS at 1.5 T than at 3 T, exceeding the threshold of 15%. In four other areas, higher BS at 1.5 T were observed as well, but all clusters were smaller than 0.08 ml.

The distribution of optimal parameters followed a similar coarse spatial pattern, being similar at 3 T (Fig. 2) and 1.5 T (Fig. 3). Roughly speaking, negative z-shimming gradient moments were optimal for dropout areas superior to $z = -30 \text{ mm}$, positive moments for dropout areas inferior to $z = -30 \text{ mm}$. For example, negative z-shimming gradient moments were required for the OFC and rACC ($z = -18 \text{ mm}$), and posterior inferior temporal gyri ($z = -18 \text{ mm}$). Positive z-shimming moments were optimal for parts of the temporal poles, amygdalae, anterior part of the inferior temporal gyri, hippo- and parahippocampus ($z = -30 \text{ mm}$). The z-shimming moments were similar for both PE polarities.

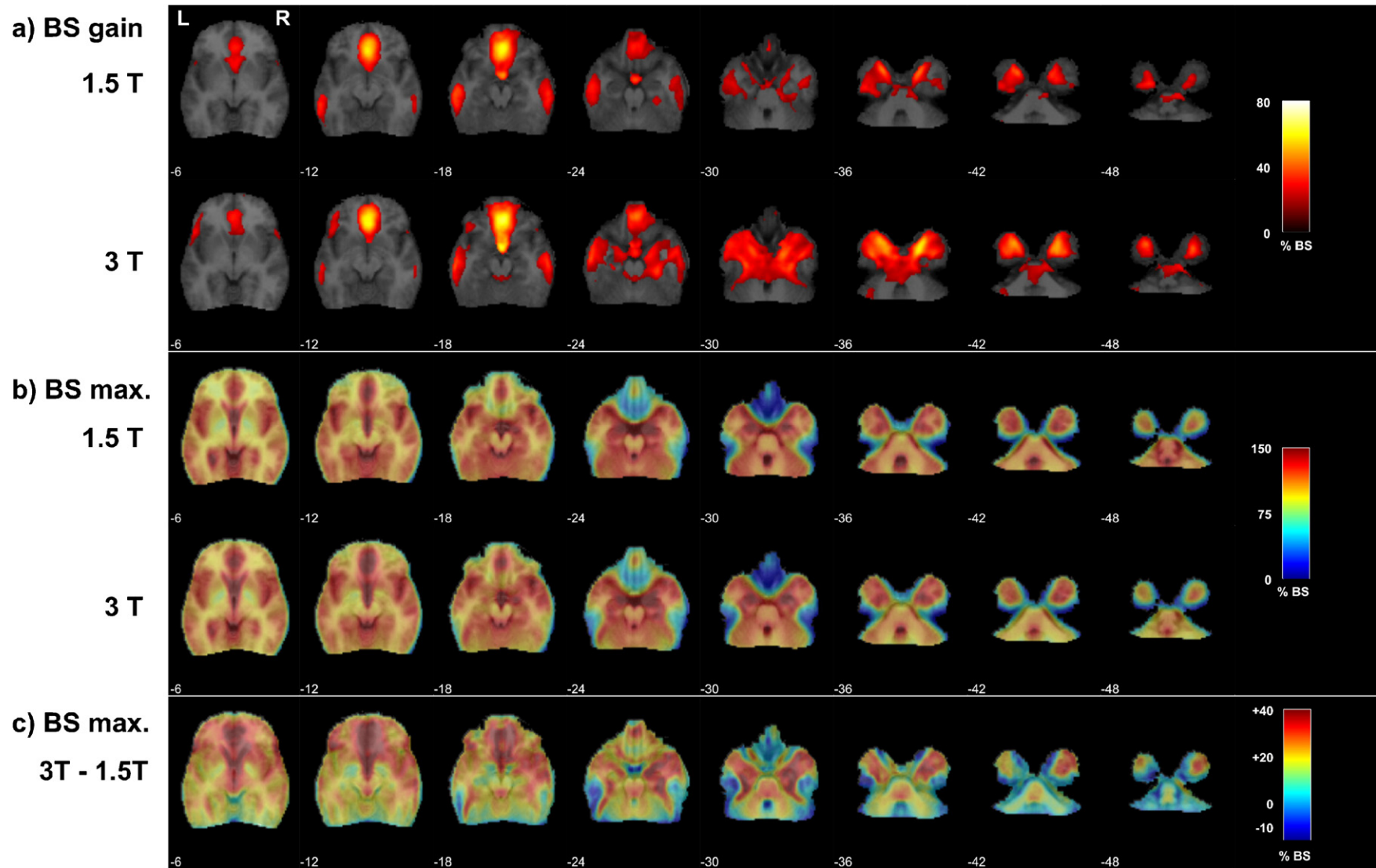


Fig. 1. BOLD sensitivity (BS) at 1.5 T and 3 T using optimal EPI parameters. All maps are superimposed over axial slices of the group mean anatomical image (z-coordinates at the lower left). Areas not scanned in all subjects and non-brain areas are excluded. (a) BS gain. Difference between the maximal BS using optimal EPI parameters and the BS achieved with standard EPI parameters (threshold >15%). The difference is scaled to the mean BS (=100%) in a well-shimmed brain area using standard EPI parameters. (b) BS max. Maximal BS using optimal EPI parameters. Same scaling as in (a). (c) Difference between the BS at 3 T and 1.5 T. Same scaling as in (a), but the BS values at 3 T have been rescaled by 1.2, to adjust for the generally higher BS expected at 3 T.

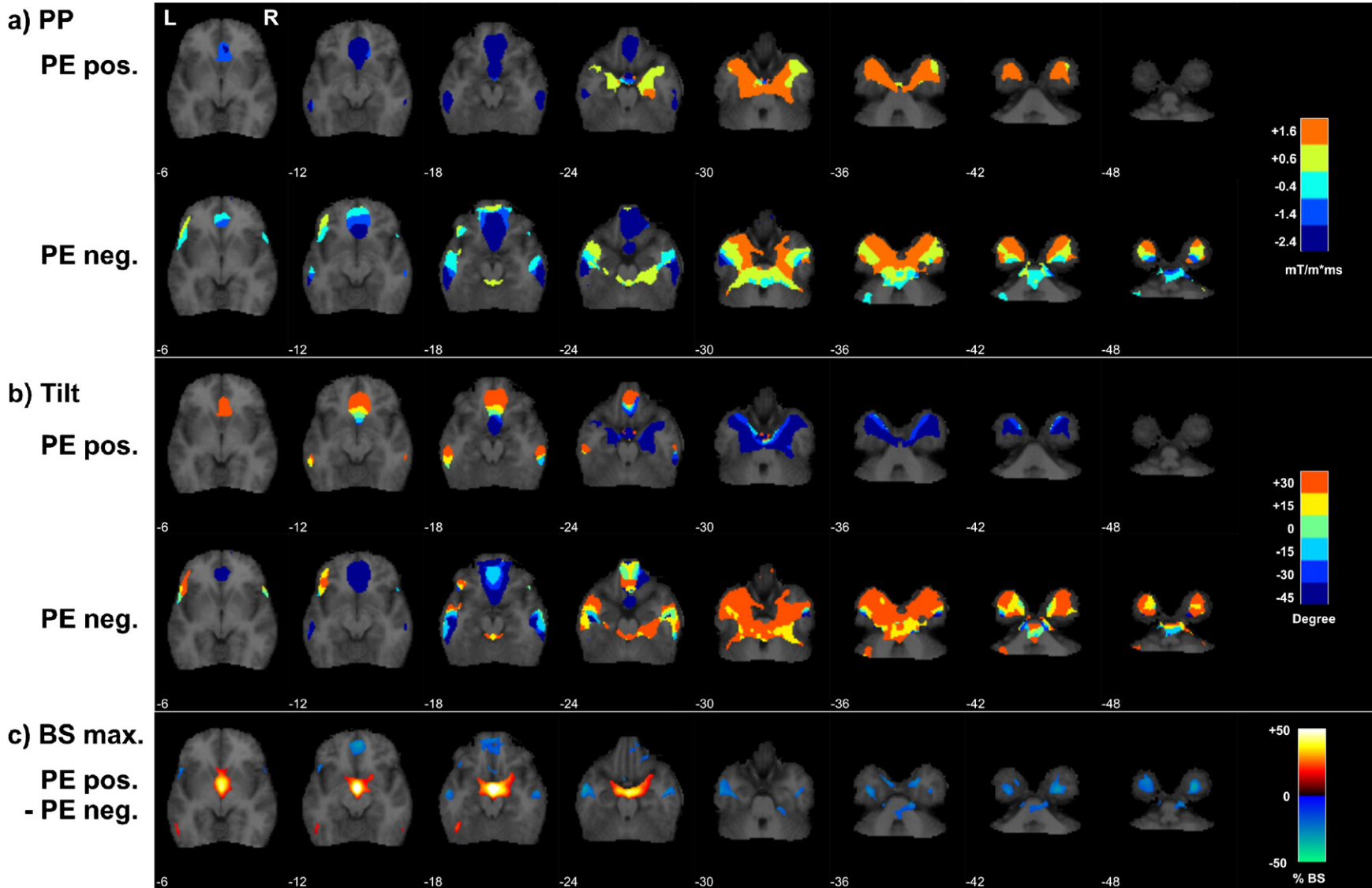


Fig. 2. Optimal EPI parameters at 3 T. All maps are superimposed over axial slices of the group mean anatomical image (z-coordinates at the lower left). Areas not scanned in all subjects and non-brain areas are excluded. Parameters are only shown for BOLD sensitivity (BS) gains exceeding 15%. (a) Optimal moment of the z-shimming prepulse (PP) given for each phase-encoding (PE) polarity. (b) Optimal slice tilt given for each PE polarity. (c) Difference between the BS using the positive and the negative PE polarity. The difference is scaled to the mean BS (= 100%) in a well-shimmed brain area using standard EPI parameters.

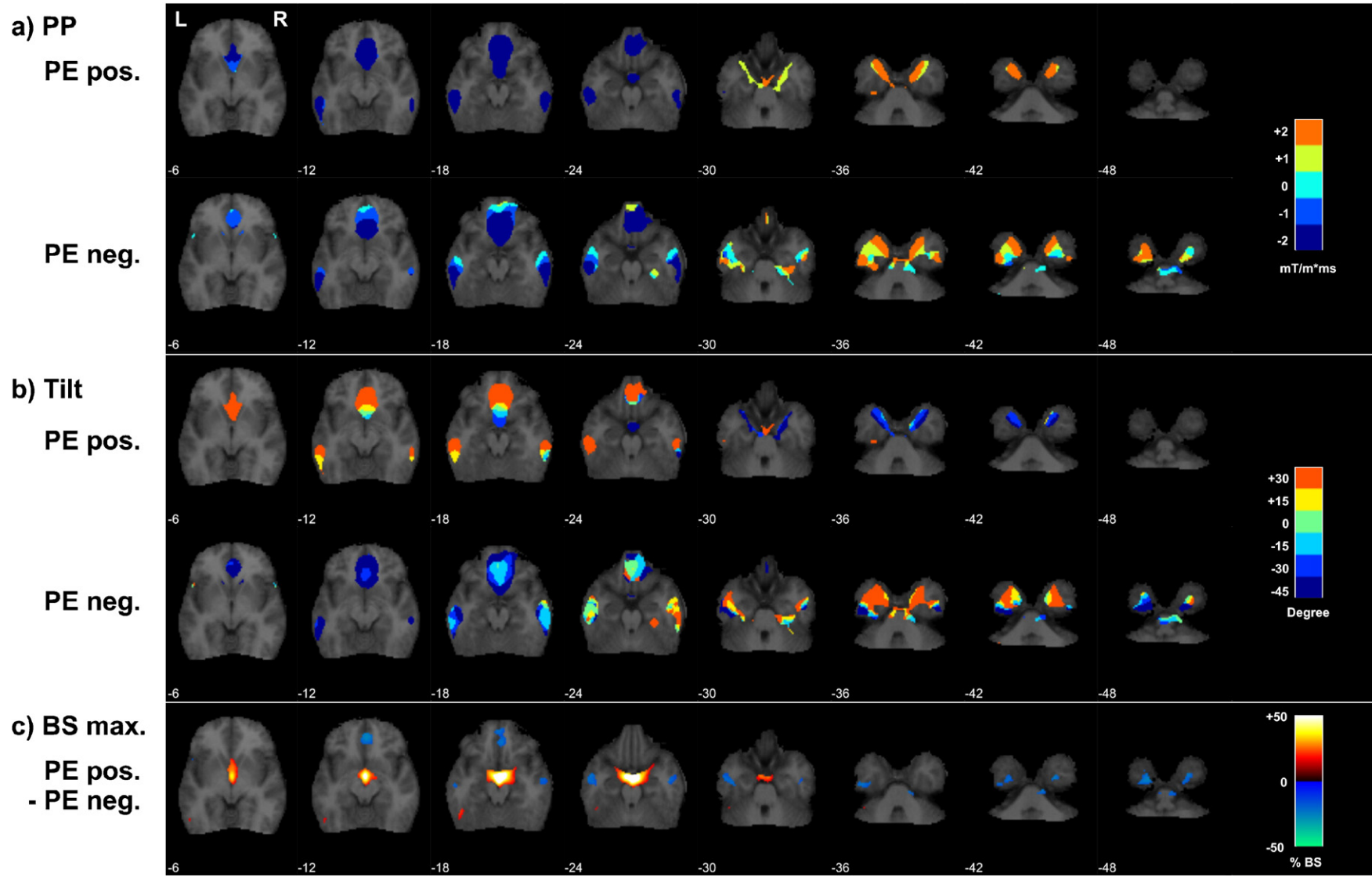


Fig. 3. Optimal EPI parameters at 1.5 T. All maps are superimposed over axial slices of the group mean anatomical image (z -coordinates at the lower left). Areas not scanned in all subjects and non-brain areas are excluded. Parameters are only shown for BOLD sensitivity (BS) gains exceeding 15%. (a) Optimal moment of the z -shimming prepulse (PP) given for each phase-encoding (PE) polarity. (b) Optimal slice tilt given for each PE polarity. (c) Difference between the BS using the positive and the negative PE polarity. The difference is scaled to the mean BS (=100%) in a well-shimmed brain area using standard EPI parameters.

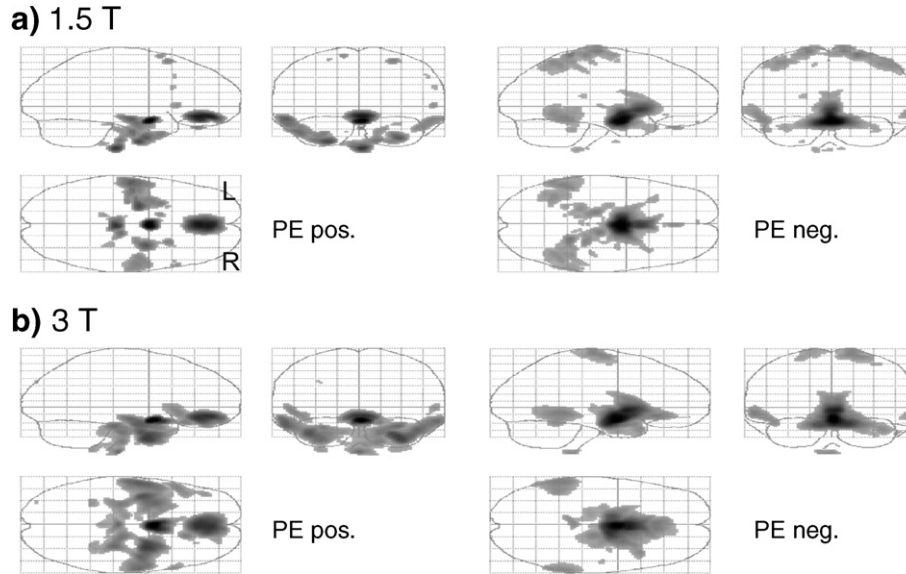


Fig. 4. Contribution of slice tilt and phase-encoding (PE) polarity to the gain in BOLD sensitivity (BS). Glass brains (maximum intensity projections) show the additional gain in BS that can be achieved by simultaneously optimizing the slice orientation, the PE direction, and the z-shimming gradient moment, rather than optimizing the z-shimming moment only with fixed slice orientation (axial) and fixed PE direction (both directions shown): at (a) 1.5 T and (b) 3 T. Only differences greater than 20% are shown.

The optimal slice tilt showed a more heterogeneous spatial pattern (Fig. 2b). For a positive PE, negative slice tilts were optimal in the temporal pole ($z=-42$ mm) and posterior OFC ($z=-18$ mm), whereas positive slice tilts were optimal in the anterior OFC and inferior temporal gyri ($z=-18$ mm). In most regions, the sign of the slice tilt changed with the PE polarity.

Figs. 2c and 3c show that positive PE polarities improved BS in the posterior OFC and caudate nuclei ($z=-6$ mm), whereas negative PE polarities improved the BS in the anterior OFC ($z=-18$ mm), parts of the fusiform gyri (around $z=-42$ mm), temporal poles ($z=-44$ mm), and inferior and middle temporal gyri ($z=-30$ mm).

Fig. 4 shows the additional BS gain that can be achieved by simultaneously optimizing the slice orientation, the PE direction, and the z-shimming prepulse moment, rather than optimizing the latter only with fixed slice orientation and fixed PE direction. The shown values correspond to the difference of the maximally achievable BS when optimizing all parameters, minus the maximally achievable BS when optimizing the z-shimming moment with a fixed slice tilt of 0° and a positive/negative PE polarity.

Region of interest analysis: optimal EPI parameters for a brain region

Tables 1 and 2 show that in all regions of interest the mean BS was improved by an optimal parameter choice. Increases in the BS were in general smaller at 1.5 T (Table 2) than at 3 T (Table 1). The most consistent increase in mean BS was observed for the mOFC+rACC, exceeding 15% at 3 T and 1.5 T. In Fig. 5a the histograms of the BS distribution of voxels in the mOFC+rACC for the optimized and standard EPI are plotted. They show that the increase in mean BS is achieved both by increasing the number of voxels with $BS > 120\%$ and also decreasing the number of voxels with $BS < 75\%$. Therefore, the increase in mean BS is not only a result of increasing the BS in voxels with a high baseline BS, but also due to a significant reduction in the number of voxels with a low BS. At 3 T, prominent BS increases were found additionally in the temporal poles (16%, Table 1) and the amygdalae (14%, Table 1). The optimal z-shimming moments for regions did not exceed the range from +1 mT/m ms to -1.4 mT/m ms, although for single voxels the optimal values were occasionally larger (e.g., Fig. 2a,

Table 1
Optimal EPI parameters for regions of interest at 3 T

Region of interest	PP [mT/m*ms]	Tilt [deg]	PE	Optimal mean % BS	Standard mean % BS
mOFC+rACC	-1.4	-45	neg.	99.2	83.5
Inferior temporal lobes	-0.4	+30	neg.	78.1	75.1
Temporal poles	+0.6	+30	neg.	106.0	89.5
Amygdala	+0.6	-45	pos.	120.9	107.3
Hippocampus+ Parahippocampus	+0.6	-45	pos.	121.9	109.7

PP=z-shimming prepulse gradient moment; PE=phase-encoding polarity; BS=BOLD sensitivity; mOFC+rACC=medial orbitofrontal cortex and rostral-ventral anterior cingulate cortex with $z < 0$ mm (MNI).

Table 2
Optimal EPI parameters for regions of interest at 1.5 T

Region of interest	PP [mT/m*ms]	Tilt [deg]	PE	Optimal mean % BS	Standard mean % BS
mOFC+rACC	-1.0	-45	neg.	91.6	76.4
Inferior temporal lobes	-1.0	+30	pos.	84.1	80.4
Temporal poles	+1.0	+30	neg.	105.8	98.5
Amygdala	+0.0	-45	pos.	120.3	115.0
Hippocampus+ Parahippocampus	+0.0	-45	pos.	122.7	118.3

PP=z-shimming prepulse gradient moment; PE=phase-encoding polarity; BS=BOLD sensitivity; mOFC+rACC=medial orbitofrontal cortex and rostral-ventral anterior cingulate cortex with $z < 0$ mm (MNI).

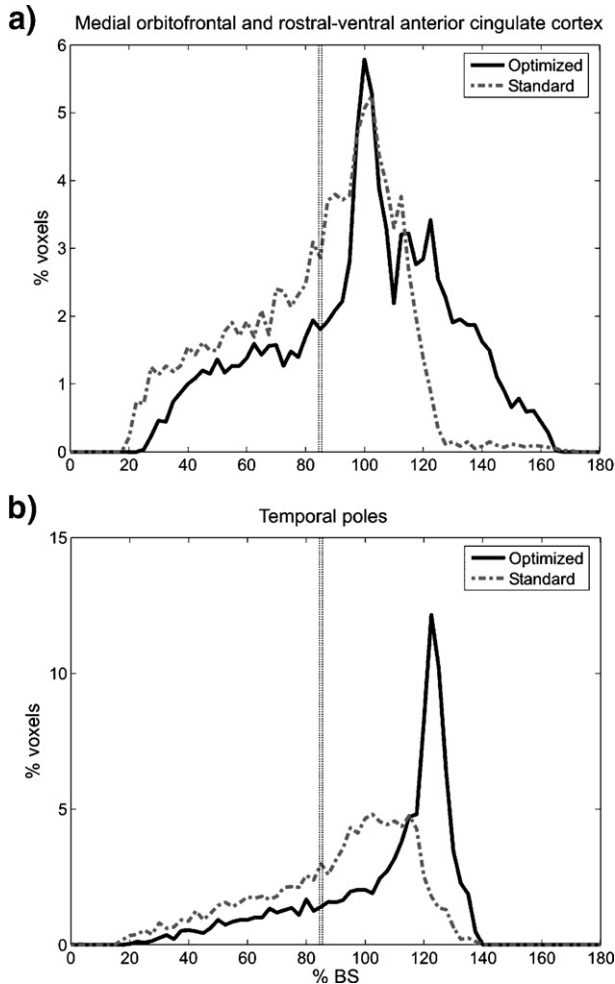


Fig. 5. EPI parameter optimization for regions of interest at 3 T: BOLD sensitivity (BS) histograms. The distribution of BS of the voxels inside (a) the medial orbitofrontal cortex and rostral–ventral anterior cingulate cortex, and (b) the temporal poles is plotted for the optimal parameters (solid black line) and standard parameters (dashed dotted gray line). For visual guidance the vertical double line marks a BS of 85%, indicating a significantly reduced BS. The BS in each voxel is scaled to the mean BS (=100%) in a well-shimmed brain area using standard EPI parameters.

$z = -18$ mm). The BS gain was only slightly increased (by less than 1.1%) for any of the ROIs when optimizing the parameters for each subject individually instead of using a single optimal parameter set for the whole group.

Optimizing parameters for a given ROI also affected the BS in the rest of the brain. To illustrate this effect, Fig. 6 shows maximum intensity projections (MIPs) of BS gains and losses across the whole brain when using the optimal parameters for the mOFC+rACC, inferior temporal lobes, and temporal poles at 3 T. The BS losses and gains exceeded 20% in many voxels across the brain. For example, when using the optimal parameters for investigation of the temporal poles, the BS in these areas increased (Fig. 6c, left), but there were BS losses in the posterior OFC and rACC (Fig. 6c, right). Fig. 7 presents single subject BS maps in different brain areas, using the standard EPI sequence (left), and a sequence with parameters that were optimized for the respective area (right).

Discussion

This study provides guidelines for maximizing the BOLD sensitivity (BS) of echo-planar imaging (EPI) in brain areas affected by signal dropout at 3 T and 1.5 T. It expands upon a previously established dropout compensation technique (De Panfilis and Schwarzbauer, 2005; Deichmann et al., 2003) focusing on the optimal choice of the slice tilt, phase-encoding (PE) direction, and z-shimming gradient moment and using otherwise conventional basic EPI parameters (echo time $TE = 30/50$ ms at 3 T/1.5 T; voxel size $3 \times 3 \times 2$ mm³). The appropriate choice of slice tilt and PE polarity primarily reduces BS loss due to susceptibility-induced gradients in the PE direction. Moderate z-shimming reduces signal loss due to through-plane gradients.

BOLD sensitivity and optimal EPI parameters

Since the direction and magnitude of the susceptibility-induced gradient varies across the brain, the optimal EPI parameters are location dependent. We have computed maps of optimal parameters for each voxel in the brain (Figs. 2 and 3) and show that, in single voxels (Fig. 1a, $z = -18$ mm), an optimal choice of parameters can increase the BS by more than 60% compared to conventional EPI (100% = baseline EPI BS in well-shimmed areas). However, full recovery of the BS is not possible in all regions, because we are limited to the application of a constant moderate z-shimming gradient moment so that BS loss is restricted in well-shimmed areas (<15% of baseline EPI BS) and high temporal resolution is retained (Deichmann et al., 2003). Also, the compensation technique does not counteract susceptibility-induced gradients in the EPI readout (RO) direction (Weiskopf et al., 2005a). Regardless of the parameter choice, areas of large residual BS loss persist, mainly confined to the OFC and inferior temporal lobes (Fig. 1b, $z = -24$ to -30 mm).

At 3 T and 1.5 T we observed similar patterns of optimal parameters (Figs. 2 and 3; Tables 1 and 2). This is not surprising, because we expect the spatial distribution of the field inhomogeneities to be similar and to differ mainly in its magnitude (scaled by the static magnetic field).

Approximately speaking, negative z-shimming gradient moments were optimal for dropout areas superior to $z = -30$ mm, and positive moments for dropout areas inferior to $z = -30$ mm (Figs. 2a and 3a). For example, the temporal poles, amygdalae, hippocampus and parahippocampus all benefit from positive z-shimming moments, and the OFC from a negative one. Positive PE polarities improved BS in the posterior OFC and caudate nuclei, whereas negative PE polarities improved BS in the anterior OFC, and parts of the inferior temporal lobes (Figs. 2c and 3c). The optimal slice tilt parameter showed a more heterogeneous spatial pattern (Figs. 2b and 3b). For the positive PE polarity, negative slice tilts were optimal in the temporal pole and posterior OFC, and positive slice tilts in the anterior OFC and inferior temporal gyri. In most brain regions, the sign of the optimal slice tilt reversed together with the PE polarity. The data support the assumption that simultaneous optimization of z-shimming moment, slice tilt, and PE polarity leads to an improved recovery of BS losses, compared to the optimization of only one parameter. As an example, it is shown that only optimizing the z-shimming moment does not yield the same BS gains as optimizing all three parameters (Fig. 4).

Since many investigators using fMRI are interested in brain regions extending over larger areas, we determined parameter sets optimizing the mean BS for a variety of regions of interest (ROI);

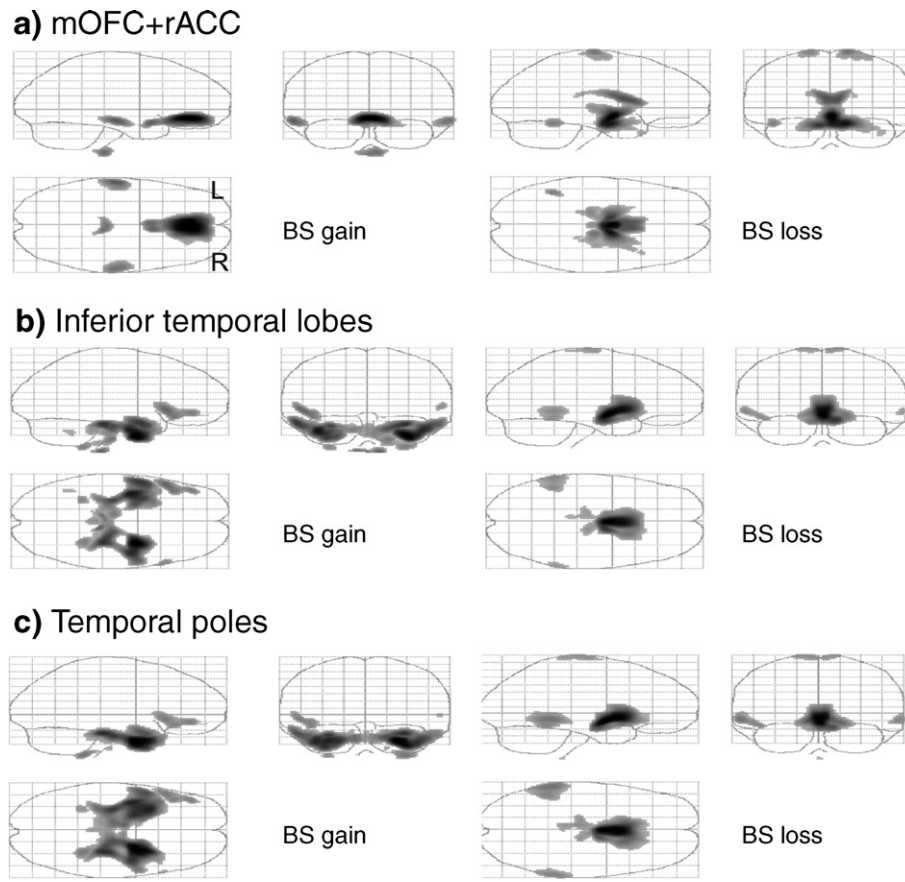


Fig. 6. BOLD sensitivity (BS) gains and losses when applying parameter sets optimized for (a) medial orbitofrontal cortex and rostral–ventral ACC (mOFC+rACC), (b) inferior temporal lobes, (c) temporal poles. Left column of glass brains (maximum intensity projections) shows the gains in BS using the optimized parameters compared to the standard EPI scan, while the right column shows the accompanying losses. Only differences greater than 20% are shown.

see Tables 1 and 2): the medial OFC (mOFC) and rostral–ventral anterior cingulate cortex (rACC); the inferior temporal lobes; temporal poles; amygdalae; and hippo- and parahippocampal region. The most prominent mean BS recovery (approximately 15%) was achieved in the mOFC+rACC, reflecting the extended area of dropout in this region. At 3 T, a considerable BS gain was also achieved in the temporal poles (16%) and the amygdalae (14%). The smaller increase of the mean BS in the other ROIs was most likely caused by partial volume effects. Nevertheless, the gain may be very significant in single voxels or parts of these areas and sensitivity loss is restricted to a worst case of 15% in well-shimmed areas. Obviously, the optimization must be redone if one is interested in a smaller subpart of the ROIs or altered ROIs.

Comparison of 3 T and 1.5 T

In general, the increases in BS using optimal EPI parameters were more substantial at 3 T than at 1.5 T, as can be seen, for example, in the temporal lobes (Fig. 1a, $z = -36$ mm) or from the larger BS increases in the selected regions of interest (Tables 1 and 2). The higher effectiveness of the dropout compensation at 3 T supports the notion that 3 T may retain its generally higher BS compared to 1.5 T even in areas affected by susceptibility-induced gradients. Based on literature values for typical increases in BS going from 1.5 T to 3 T (Hoenig et al., 2005; Triantafyllou et al., 2005; Turner et al., 2005), one can conservatively estimate a lower

limit of about 20% BS increase in well-shimmed areas and rescale the BS maps accordingly. Using such recalibrated BS maps, a direct comparison between the two field strengths is possible and suggests that 3 T provides a higher BS than 1.5 T in most brain areas (Fig. 1c). Thus, fMRI at higher fields in areas affected by susceptibility-induced gradients benefits more from dropout compensation techniques and so any comparison of BS between different field strengths should consider these techniques to avoid a potential bias. However, we advise caution. We did not directly measure and compare BS, but linked one set of results to the other on the basis of literature values. Moreover, the 3 T scanner was equipped with a head gradient system enabling a very rapid EPI readout.

Limitations and considerations

We took particular care to accurately estimate the BS from single-shot image data. All images were corrected for geometric distortions, which can otherwise simulate signal loss by shifting signal from one area into other areas. Distortion-induced intensity modulations were not corrected, because the correction can reduce the signal-to-noise ratio (SNR; Hutton et al., 2002). However, in GE EPI these intensity modulations are expected to be significantly smaller than the signal loss caused by the intravoxel dephasing. Importantly, our BS estimate was based not only on the measured signal amplitude but also took local echo time shifts (Deichmann et

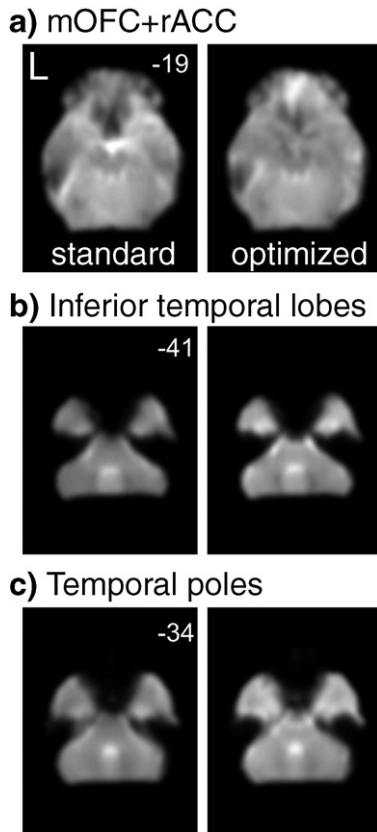


Fig. 7. Exemplary BOLD sensitivity (BS) maps of standard EPI (left) and EPI optimized (right) for scanning the (a) medial orbitofrontal cortex and rostral–ventral anterior cingulate cortex (mOFC+rACC), (b) inferior temporal lobes, and (c) temporal poles at 3 T. Smoothed single subject BS estimates are presented as axial slices (z -coordinates indicated in the upper right corner). Areas not scanned for all slice tilts are excluded.

al., 2002) caused by susceptibility-induced gradients in the PE direction into account.

Since we performed neither an fMRI experiment nor acquisition of a time-series of images to estimate BS and temporal noise (including physiological noise components; e.g., Krüger et al., 2001), the reported BS values should be interpreted with particular care regarding possible temporal noise variations. For example, regions close to contrast edges may suffer from motion artifacts and regions close to larger vessels from cardiac artifacts. Scanner instability and the Nyquist ghosting in EPI (Josephs et al., 2006) can be another source of temporal noise. In these cases the BS based only on thermal noise may be overestimated. The BS values were measured relative to the BS in a well-shimmed area in a conventional EPI. Since the reference value is the average BS in a large ROI, signals from different types of brain tissue (gray, white matter, cerebrospinal fluid) are mixed. A spatial variation in their relative density can therefore be misinterpreted as a different BS. Similarly, variations in the RF coil sensitivity and B_1 field inhomogeneities can influence the estimation of the local BS. A non-uniformity of calculated BS values across the brain due to different local coil sensitivities or different relative tissue densities may complicate the comparison of BS in different brain areas and bias the estimation of optimal parameters for extended ROIs. However, the variations would not affect the estimation of the optimal parameter maps, because they are constant within a single voxel for all parameters.

This study was based on a group of 5 subjects instead on a single subject, to provide a more representative estimate of the BS. We regarded it as reasonable to pool multiple subjects, because the relatively similar head orientation of the subjects in the scanners (standard deviation of head tilt $<5^\circ$) will generate similar field inhomogeneities. Any small variation in pitch is expected to yield similar BS changes as the corresponding change in the slice tilt (Deichmann et al., 2003). The similar head orientation also allows for a fixed spatial coordinate system based on the scanner to define the slice tilts, instead of using different individual head coordinate systems. Obviously, our results pertain only to this (common) positioning. The pooling of multiple subjects is further supported by the result that the mean BS gains in all ROIs did not significantly increase (by less than 1.1%) when the parameters were optimized for each subject individually instead of using a single optimal parameter set for the whole group.

The group analysis required spatial normalization and smoothing of the data. As in all group analyses, both the reduced effective spatial resolution and the inter-individual differences in brain anatomy make it difficult to locate and delineate small brain structures. This may impair extracting optimal parameters for small regions or exact delineation and separation of different regions. Similarly, since the regions of interest investigated in this study are mainly based on the single-subject AAL atlas (Tzourio-Mazoyer et al., 2002), the derived parameters are subject to mismatch between individual anatomies and so should be regarded only as approximate guidelines. More reliable estimates with error margins may be possible with the increased availability of cytoarchitectonic probability maps, such as the one used to define the amygdala (Amunts et al., 2005).

Only a subset of possible EPI acquisition parameters was studied. Firstly, only axial and oblique axial slice orientations with left–right readout gradient direction were considered. This is reasonable, because these are the most frequently used for fMRI and allow for the fastest acquisition, where peripheral nerve stimulation is a limitation. Secondly, only moderate z -shimming moments were allowed to avoid widespread signal loss in well-shimmed areas. In fact, because of technical problems the maximal negative z -shimming moment was slightly larger at 3 T than at 1.5 T which may have contributed to the larger BS gains we observed at 3 T in the OFC. Thirdly, slice tilts were limited to less than 45° , because special care must be taken with large slice tilts, in particular positive ones (positive values denote tilts of the anterior edge of the slice towards the feet measured from the axial plane). In this case the slice may intersect with the oral cavity and nose, causing wrap over, chemical shift artifacts (from unsuppressed fatty tissue signals) and larger Nyquist ghost. Therefore, we would recommend using negative slice tilts if possible. Another solution may be to saturate the signal from these areas or to use 3D spatially selective RF excitation pulses.

The presented dropout compensation is particularly useful for recovering BS where two or more regions are affected by similar susceptibility-induced gradients. If two different regions require opposite z -shimming moments, the optimal parameter set for one region can significantly reduce the BS (by much more than 15%) for the other brain region (see Fig. 6 and Deichmann et al., 2003). Our whole-brain maps help to identify such situations. They can even help to overcome the problem by calibrating slice-dependent z -shimming (Weiskopf and Deichmann, 2006). Slice-dependent z -shimming uses the optimal gradient moment for each region separately (Cordes et al., 2000), at least where they can be segregated in the slice select direction.

General applicability: scanner and sequence parameters

Since our imaging data were acquired on two particular MRI scanner setups, it should be checked whether the specific results and guidelines are applicable for a different scanner setup. For example both scanners were equipped with second order shim coils and the manufacturer's automatic 3D shim was performed prior to the EPI acquisition. If only first order shims are available, the BS may be reduced. The 3 T scanner was operated with a head gradient system enabling a very rapid EPI readout.

The mean head position in the scanner should be measured for a group of subjects, in order to ensure that the tilt angles are comparable. Any differences in head tilts are most likely about the *x*-axis (pitch). A small difference in pitch may be approximated by the corresponding slice tilt (Deichmann et al., 2003) and the optimal slice tilts may be adjusted accordingly.

The EPI sequence parameters should be chosen to be as similar as possible. For example, longer echo times require proportionally increased z-shimming gradient moments (Deichmann et al., 2003). However, despite the application of an increased z-shimming gradient moment BS loss may still be increased for longer echo times due to in-plane susceptibility-induced gradients.

If an increased slice thickness is used, the gradient moment must be reduced reciprocally to avoid excessive BS losses due to dephasing in well-shimmed brain areas (Deichmann et al., 2003). However, we would not advise to use thicker slices because the reduced z-shimming gradient moment and larger slice thickness will both yield significantly larger BS losses in areas affected by field inhomogeneities.

A change in the EPI readout time (echo spacing) and a change in the in-plane resolution will both affect the BS loss due to in-plane susceptibility-induced gradients. Increasing the in-plane resolution (extending k-space coverage) will reduce both dropouts due to susceptibility-induced gradients in the readout (Weiskopf et al., 2005a) and PE direction (Deichmann et al., 2002), if the readout time and other sequence parameters are kept constant. On the other hand, an increased resolution will generally reduce the signal-to-noise ratio (SNR) and thus the BS in well-shimmed areas (Merboldt et al., 2000).

However, often the readout time is increased with a higher spatial resolution. An increased readout time will primarily affect dropouts due to susceptibility-induced gradients in the PE direction. The increased readout time will increase any shifts to longer effective echo times and exacerbate dropouts due to the shift of the echo outside the acquisition window (Deichmann et al., 2002). Paradoxically, a longer readout time may reduce the BS losses that are caused by shifts to smaller effective echo times, because the readout starts earlier after the RF excitation. However, this type of BS loss occurs only for significantly higher field distortions in the PE direction (Deichmann et al., 2003) and is rare. A longer readout time will also yield larger geometric distortions (Hutton et al., 2002). The readout time may also be increased when using a lower receiver bandwidth, causing the same problems. However, lower bandwidths increase the SNR and BS (Zou et al., 2005).

For other principal imaging orientations (i.e., sagittal or coronal) or different PE directions (e.g., left–right), it would be very difficult if not impossible to extrapolate optimal parameters from the results presented here. However, other studies assessed effects of different principal imaging orientations on BS, for example for the amygdala (Chen et al., 2003; Robinson et al., 2004; Merboldt et al., 2001). One should be aware that geometric

distortions depend on the PE direction (Bowtell et al., 1994; Weiskopf et al., 2005b) and may compromise direct comparisons between studies acquired with different PE directions, unless they are corrected for.

Conclusion

This paper provides guidelines for optimizing echo-planar imaging (EPI) for functional imaging studies in regions affected by susceptibility-induced BOLD sensitivity (BS) losses at two field strengths (1.5 T and 3 T). Whole-brain maps show the slice tilt, phase-encoding (PE) polarity, and z-shimming gradient moment that maximize the BS in each voxel. Furthermore, optimal parameters are reported for selected regions of interest extending across larger areas (e.g., the medial orbitofrontal cortex). The maps can be used to assess the feasibility and to optimize fMRI of regions affected by BS loss. The maps can also help in choosing which field strength may be optimal.

Acknowledgments

This study was supported by the Wellcome Trust. We thank S.B. Eickhoff for the help with extracting cytoarchitectonic probability maps from the SPM Anatomy toolbox and J. O'Doherty for providing his expertise on neuroanatomy.

References

- Amunts, K., Kedo, O., Kindler, M., Pieperhoff, P., Mohlberg, H., Shah, N.J., Habel, U., Schneider, F., Zilles, K., 2005. Cytoarchitectonic mapping of the human amygdala, hippocampal region and entorhinal cortex: intersubject variability and probability maps. *Anat. Embryol.* 210, 343–352.
- Andersson, J.L.R., Hutton, C., Ashburner, J., Turner, R., Friston, K., 2001. Modeling geometric deformations in EPI time series. *NeuroImage* 13, 903–919.
- Ashburner, J., Friston, K.J., 1999. Nonlinear spatial normalization using basis functions. *Hum. Brain Mapp.* 7, 254–266.
- Bowtell, R.W., McIntyre, D.J.O., Commandre, M.-J., Glover, P.M., Mansfield, P., 1994. Correction of geometric distortion in echo planar images. *Proc. SMR, 2nd Annual Meeting, Society of Magnetic Resonance, Berkeley, CA, USA*, p. 411.
- Chen, N.K., Dickey, C.C., Yoo, S.S., Guttmann, C.R., Panych, L.P., 2003. Selection of voxel size and slice orientation for fMRI in the presence of susceptibility field gradients: application to imaging of the amygdala. *NeuroImage* 19, 817–825.
- Cho, Z.H., Ro, Y.M., 1992. Reduction of susceptibility artifact in gradient-echo imaging. *Magn. Reson. Med.* 23, 200.
- Collins, D.L., Neelin, P., Peters, T.M., Evans, A.C., 1994. Automatic 3D intersubject registration of MR volumetric data in standardized Talairach space. *J. Comput. Assist. Tomogr.* 18, 192–205.
- Cordes, D., Turski, P.A., Sorenson, J.A., 2000. Compensation of susceptibility-induced signal loss in echo-planar imaging for functional applications. *Magn. Reson. Imaging* 18, 1055–1068.
- Deichmann, R., Josephs, O., Hutton, C., Corfield, D.R., Turner, R., 2002. Compensation of susceptibility-induced BOLD sensitivity losses in echo-planar fMRI imaging. *NeuroImage* 15, 120–135.
- Deichmann, R., Gottfried, J.A., Hutton, C., Turner, R., 2003. Optimized EPI for fMRI studies of the orbitofrontal cortex. *NeuroImage* 19, 430–441.
- Deichmann, R., Schwarzbauer, C., Turner, R., 2004. Optimisation of the 3D MDEFT sequence for anatomical brain imaging: technical implications at 1.5 and 3 T. *NeuroImage* 21, 757–767.
- De Panfilis, C., Schwarzbauer, C., 2005. Positive or negative blips? The effect of phase encoding scheme on susceptibility-induced signal losses in EPI. *NeuroImage* 25, 112–121.

- Devlin, J.T., Russell, R.P., Davis, M.H., Price, C.J., Wilson, J., Moss, H.E., Matthews, P.M., Tyler, L.K., 2000. Susceptibility-induced loss of signal: comparing PET and fMRI on a semantic task. *NeuroImage* 11, 589–600.
- Eickhoff, S.B., Stephan, K.E., Mohlberg, H., Grefkes, C., Fink, G.R., Amunts, K., Zilles, K., 2005. A new SPM toolbox for combining probabilistic cytoarchitectonic maps and functional imaging data. *NeuroImage* 25, 1325–1335.
- Frahm, J., Merboldt, K.D., Hänicke, W., 1988. Direct FLASH MR imaging of magnetic field inhomogeneities by gradient compensation. *Magn. Reson. Med.* 6, 480.
- Friston, K.J., Ashburner, J., Frith, C.D., Poline, J.-B., Heather, J.D., Williams, S.C., Frackowiack, R.S.J., 1995. Spatial registration and normalization of images. *Hum. Brain Mapp.* 2, 165–189.
- Friston, K.J., Harrison, L., Penny, W., 2003. Dynamic causal modelling. *NeuroImage* 19, 1273–1302.
- Hoenig, K., Kuhl, C.K., Scheef, L., 2005. Functional 3.0-T MR assessment of higher cognitive function: are there advantages over 1, 5-T imaging? *Radiology* 234, 860–868.
- Hsu, J.-J., Glover, G.H., 2005. Mitigation of susceptibility-induced signal loss in neuroimaging using localized shim coils. *Magn. Reson. Med.* 53, 243–248.
- Hutton, C., Bork, A., Josephs, O., Deichmann, R., Ashburner, J., Turner, R., 2002. Image distortion correction in fMRI: a quantitative evaluation. *NeuroImage* 16, 217–240.
- Hutton, C., Deichmann, R., Turner, R., Andersson, J.L.R., 2004. Combined correction for geometric distortion and its interaction with head motion in fMRI. *Proceedings of ISMRM 12*, Kyoto, Japan, p. 1084.
- Jezzard, P., Balaban, R.S., 1995. Correction for geometric distortion in echo planar images from B0 field variations. *Magn. Reson. Med.* 34, 65–73.
- Josephs, O., Turner, R., Friston, K., 1997. Event-related fMRI. *Hum. Brain Mapp.* 5, 243–248.
- Josephs, O., Deichmann, R., Turner, R., 2000. Trajectory measurement and generalised reconstruction in rectilinear EPI. *Proceedings of ISMRM 8*, Denver, Colorado, USA, p. 1517.
- Josephs, O., Weiskopf, N., Deichmann, R., 2006. Correction of EPI Nyquist ghosting caused by the non-uniform frequency response of the MRI receiver chain. *Proceedings of ISMRM 14*, Seattle, Washington, USA.
- Krüger, G., Kastrup, A., Glover, G.H., 2001. Neuroimaging at 1.5 T and 3.0 T: comparison of oxygenation-sensitive magnetic resonance imaging. *Magn. Reson. Med.* 45, 595–604.
- Logothetis, N.K., 2003. MR-imaging in the non-human primate: studies of function and of dynamic connectivity. *Curr. Opin. Neurobiol.* 13, 630–642.
- Merboldt, K.D., Finsterbusch, J., Frahm, J., 2000. Reducing inhomogeneity artifacts in functional MRI of human brain activation-thin sections vs. gradient compensation. *J. Magn. Reson.* 145, 184–191.
- Merboldt, K.D., Fransson, P., Bruhn, H., Frahm, J., 2001. Functional MRI of the human amygdala? *NeuroImage* 14, 253–257.
- Moonen, C.T.W., Bandettini, P.A., 2000. *Functional MRI*. Springer, Berlin.
- Ojemann, J., Akbudak, E., Snyder, A.Z., McKinstry, R.C., Raichle, M.E., Conturo, T.E., 1997. Anatomic localization and quantitative analysis of gradient refocused echo-planar fMRI susceptibility artifacts. *NeuroImage* 6, 156–167.
- Ordidge, R.J., Gorell, J.M., Deniau, J.C., Knight, R.A., Helpem, J.A., 1994. Assessment of relative brain iron concentrations using T2-weighted and T2*-weighted MRI at 3 Tesla. *Magn. Reson. Med.* 32, 335–341.
- Robinson, S., Windischberger, C., Rauscher, A., Moser, E., 2004. Optimized 3 T EPI of the amygdalae. *NeuroImage* 22, 203–210.
- Roebroeck, A., Formisano, E., Goebel, R., 2005. Mapping directed influence over the brain using Granger causality and fMRI. *NeuroImage* 25, 230–242.
- Stenger, V.A., Boada, F.E., Noll, D.C., 2000. Three-dimensional tailored RF pulses for the reduction of susceptibility artifacts in T2*-weighted functional MRI. *Magn. Reson. Med.* 44, 525–531.
- Sutton, B.P., Noll, D.C., Fessler, J.A., 2004. Dynamic field map estimation using a spiral-in/spiral-out acquisition. *Magn. Reson. Med.* 51, 1194–1204.
- Triantafyllou, C., Hoge, R.D., Krueger, G., Wiggins, C.J., Potthast, A., Wiggins, G.C., Wald, L.L., 2005. Comparison of physiological noise at 1.5 T, 3 T and 7 T and optimization of fMRI acquisition parameters. *NeuroImage* 26, 243–250.
- Turner, R., Mechelli, A., Noppeney, U., Price, C., Glensman, J., Rombouts, S., Veltman, D., 2005. A comparison of the effectiveness of 3 T and 1.5 T MRI scanners in a multi-subject fMRI study of visual memory. *Abstract at 11th Annual Meeting of the OHBM*, Toronto, Ontario, Canada.
- Tzourio-Mazoyer, N., Landeau, B., Papathanassiou, D., Crivello, F., Etard, O., Delcroix, N., Mazoyer, B., Joliot, M., 2002. Automated anatomical labeling of activations in SPM using a macroscopic anatomical parcellation of the MNI MRI single-subject brain. *NeuroImage* 15, 273–289.
- Weiskopf, N., Deichmann, R., 2006. Automated variable z-shim for fMRI: user-independent reduction of signal dropout in the orbitofrontal cortex and temporal lobe. *Abstract at 12th Annual Meeting of the OHBM*, Florence, Italy.
- Weiskopf, N., Hutton, C., Josephs, O., Turner, R., Deichmann, R., 2005a. Signal dropouts in EPI caused by susceptibility gradients in the frequency encoding direction: theory and experimental validation. *Abstract at 11th Annual Meeting of the OHBM*, Toronto, Ontario, Canada.
- Weiskopf, N., Klose, U., Birbaumer, N., Mathiak, K., 2005b. Single-shot compensation of image distortions and BOLD contrast optimization using multi-echo EPI for real-time fMRI. *NeuroImage* 24, 1068–1079.
- Zaitsev, M., Hennig, J., Speck, O., 2004. Point spread function mapping with parallel imaging techniques and high acceleration factors: fast, robust, and flexible method for echo-planar imaging distortion correction. *Magn. Reson. Med.* 52, 1156–1166.
- Zou, P., Hutchins, S.B., Dutkiewicz, R.M., Li, C.S., Ogg, R.J., 2005. Effects of EPI readout bandwidth on measured activation map and BOLD response in fMRI experiments. *NeuroImage* 27, 15–25.